



Nonlinear intensity difference correlation for multi-temporal remote sensing images

Shunping Ji^a, Tong Zhang^{b,*}, Qingfeng Guan^c, Junli Li^d

^a School of Remote Sensing and Information Engineering, Wuhan University, Wuhan 430079, China

^b State Key Laboratory of Information Engineering in Surveying, Mapping and Remote Sensing, Wuhan University, Wuhan 430079, China

^c Center for Advanced Land Management Information Technologies, Faculty of Geography and GIScience, School of Natural Resources, University of Nebraska – Lincoln, Lincoln, NE 68583-0973, USA

^d Xinjiang Institute of Ecology and Geography, Chinese Academy of Sciences, Urumqi 830011, China

ARTICLE INFO

Article history:

Received 24 September 2011

Accepted 15 June 2012

Keywords:

Non-linear intensity difference correlation

Multi-temporal

Multi-sensor

Image matching

Ground control points

ABSTRACT

Compared to geometric distortions exhibited in remote sensing images, radiometric deformations are less addressed in the literature and linear variations are usually assumed during image matching or registration. This paper proposes a novel robust and automatic image matching approach for multi-temporal and multi-sensor remote sensing images which usually present non-linear radiometric changes. We introduce a non-linear intensity difference correlation (NIDC) algorithm that aims to reduce the impacts of non-linear intensity differences during image matching. Differences of illumination intensity are accounted for and modeled in the NIDC algorithm through the extension of traditional feature-based matching techniques. Our proposed approach has been tested with typical multi-temporal and multi-sensor remote sensing images characterized by either dense or sparse ground control points (GCPs). Experimental results demonstrate that our matching approach outperforms common image matching techniques such as cross correlation (CC), scale-invariant feature transform (SIFT), and speeded-up robust features (SURF) with respects to matching success rate and robustness in test data.

© 2012 Elsevier B.V. All rights reserved.

1. Introduction

High resolution remote sensing imagery radically improves human's capabilities in earth observation and has been widely leveraged in many geospatial applications, such as Digital Surface Model (DSM) generation (Zhang and Gruen, 2006; Deilami and Hashim, 2011), change detection (Pacifi and Del Frate, 2010; Bouziani et al., 2010), and topographical mapping and updating (Holland et al., 2006). Such applications usually need a collection of multi-temporal images that are acquired at different times, under different imaging conditions, and by different sensors. Automatic, fast, yet reliable and robust image matching or registration is a prior and fundamental step before high-resolution imagery products can be effectively utilized. However, high-quality image matching remains a challenging problem in the domain of computer vision, Photogrammetry, and remote sensing, despite that many methods have been proposed. The essence of image matching is to establish robust correspondence between reference and new images given significant geometric and radiometric deformations. In computer vision, creating robust feature detectors and

descriptors that are fully or partially invariant to different variations (e.g. image scaling, rotation, affine transformations, illumination or view point changes) is the centerpiece for image matching. A large portion of image matching techniques focuses on the issue of achieving geometric invariance. For example, scale-invariant feature transform (SIFT) (Lowe, 2004), gradient location and orientation histogram (GLOH) (Mikolajczyk and Schmid, 2005), and speed-up robust features (SURF) (Bay et al., 2008) are both capable of finding robust features that are scale and rotation-invariant. Their usefulness has been extensively demonstrated in object recognition, 3D reconstruction, and image registration. Apart from geometric distortions, radiometric deformations, particularly non-linear illumination changes have not been extensively addressed in the literature. Many factors such as different atmospheric, seasonal, and weather conditions would cause non-linear illumination variations that complicate design and implementation of robust and reliable image matching techniques. Since the Least Square algorithm (Ackermann, 1984) been proposed, most of historical studies assume linear intensity variations during remote sensing imagery matching or registration. In computer vision, the development of most popular feature detectors and descriptors are based on the linear illumination assumption so as to reduce model complexity. Even if the negative influence of non-linear illumination variations has been recognized, only preliminary methods

* Corresponding author. Tel.: +86 27 68778969; fax: +86 27 68778969.

E-mail address: geogrid@gmail.com (T. Zhang).

are proposed to address intensity difference issues. These methods include the penalizing of large gradient values with a pre-assigned threshold (Lowe, 2004) and using of a local descriptor matrix based on GLOH (Li et al., 2011).

If accurate geo-referencing information is not available from original images, geometric deformation information has to be extracted from candidate matching points obtained by regular feature point detectors (Yu et al., 2008). The lack of accurate geo-reference information creates barriers for performing reliable precision evaluation of matched points, which is essential for remote sensing applications. Fortunately, most original commercial satellite imagery carries geometric location information to support rigorous and accurate image matching and geo-referencing. For example, Digital Surface Models (DSM) extracted from SPOT HRS stereo pairs based on their strict geometric model parameters can achieve an accuracy of 5–20 m (Peter et al., 2006) while geo-referencing accuracy of IKONOS images using the rational polynomial coefficients (RPC, provided with original image products) can reach approximately 20 m (Dial, 2000).

This paper concentrates on the issue of non-linear radiometric changes for multi-temporal and multi-sensor remote sensing images. We assume that initial approximately geometric transformation parameters between reference image and new matching images are already known. Reference images have been geo-referenced with accurate GCPs. New images are assumed to have initial geometric transformation parameters. Based on these assumptions, this paper presents an automatic and robust image matching method and focuses on non-linear intensity changes rather than geometric deformations since the later can be largely addressed through image pre-processing using geometric location models. Initial geometric transformation information is also useful for the subsequent evaluation of our image matching approach.

In this paper, a non-linear intensity difference correlation (NIDC) algorithm is proposed for the matching of multi-temporal and multi-source images. The NIDC algorithm is integrated with traditional feature matching techniques to realize highly reliable and robust image matching. Based on GCP correspondences derived from our approach, we can further compute RPC parameters and perform accuracy evaluation of positioning for new remote sensing images as accurate image geo-referencing information is available. Experiments demonstrate that our matching approach outperforms several image matching techniques proposed in the literature in terms of matching performance (i.e. correct match rates and robustness to changes).

2. Non-linear correlation of multi-temporal images

2.1. Feature-based matching techniques

Differences in seasons and imaging angles, varying illumination conditions as well as unpredictable ground object changes may introduce significant non-linear radiometric variations between image pairs. Many rotation and scale-invariant features of ground objects are robust against only a small range of image intensity changes. Theoretically, feature-based matching techniques are superior to classical area-based cross correlation methods that depend on image intensities. Nevertheless, current popular feature-based matching algorithms, including SIFT, GLOH, and SURF, are inadequate to handle non-linear intensity differences because linear illumination variations are assumed. As shown in Fig. 1, varying degrees of radiometric differences and ground object changes can be observed between four reference/new image pairs. We applied SIFT and SURF descriptors in image matching tasks and noticed that both methods fail to achieve satisfactory matching results. Non-linear intensity deformations plus relatively small GCP

patches contribute to this failure. We used linear correlation technique to these four image pairs. The derived correlation coefficients for four image pairs are only 0.35, 0.58, 0.45, and 0.27, which reveal a weak correlation between reference and new images. Thus it is difficult to determine the reasons of mismatches since radiometric variations or ground object changes can also result in mismatching. For image pair (a), two crossed roads remain unchanged in the new image. However, illumination conditions changes in a non-linear manner, justifying the small correlation value (0.35). Unlike (a), image pair (b) has a relatively high correlation coefficient (0.58) because intensity differences are uniformly distributed between two images. For pairs (c) and (d), both new images reveal distinct physical changes of ground objects. For pair (c), a small piece of farmland with high brightness disappears in the new image. There are large significant changes of farmland and roads in pair (d). These obvious physical changes of ground objects also violate the assumption of linear intensity difference.

In addition to the negative impacts of non-linear intensity change, image matching is also sensitive to potential physical changes of ground objects which are very common. If some edge features undergo significant changes, traditional matching techniques may fail.

In this paper, we examine non-linear intensity differences on the basis of traditional feature-based matching techniques. A non-linear intensity difference correlation (NIDC) algorithm is introduced to handle the non-linear intensity differences between images. Distinctiveness of extracted features and differences of illumination intensity are both accounted for and modeled in the NIDC algorithm through the extension of traditional feature-based matching techniques.

The entire work flow for our image matching approach is illustrated in Fig. 2.

2.2. Image pre-processing using RFM

Typically, an image matching procedure starts with the production of an initial set of matches (correspondences). Remote sensing image matching is distinctive from close-range image matching in that the former is more geometrically constrained. The main focus of this paper is to correctly handle the radiometric changes between images. Therefore, the pre-processing step here is to eliminate geometric deformations in new images. To take advantages of geometric information in image pre-processing, we adopt geometric models that describe the relations between original GCPs and corresponding image points in new images. Common geometric location models include strict physical models, rational function models (RFM), and orientation image models. RFM has the advantages of simplicity and generality, being applicable to many commercial satellite images. Another advantage lies in their high precision in fitting strict physical imaging models (up to 10^{-2} pixels) (Tao and Hu, 2001). In this study, we choose RFM as our uniform geometric location model and transform original parameters of geometric location models (if provided) into RPC parameters. The inverse formula of RFM that transforms ground coordinates to image coordinates can be written as

$$\begin{aligned} X &= \frac{Num_S(P, L, H)}{Den_S(P, L, H)} \\ Y &= \frac{Num_L(P, L, H)}{Den_L(P, L, H)} \end{aligned} \quad (1)$$

where (X, Y) are regularized image coordinates, (P, L, H) are regularized ground coordinates, (Num_S, Num_L) are polynomial numerators, and (Den_S, Den_L) are polynomial denominators. Details of Eq. (1) are described in (Fraser and Hanley, 2003).

Initial corresponding coordinates are predicted in new images based on original GCPs and initial RPC parameters through Eq. (1)

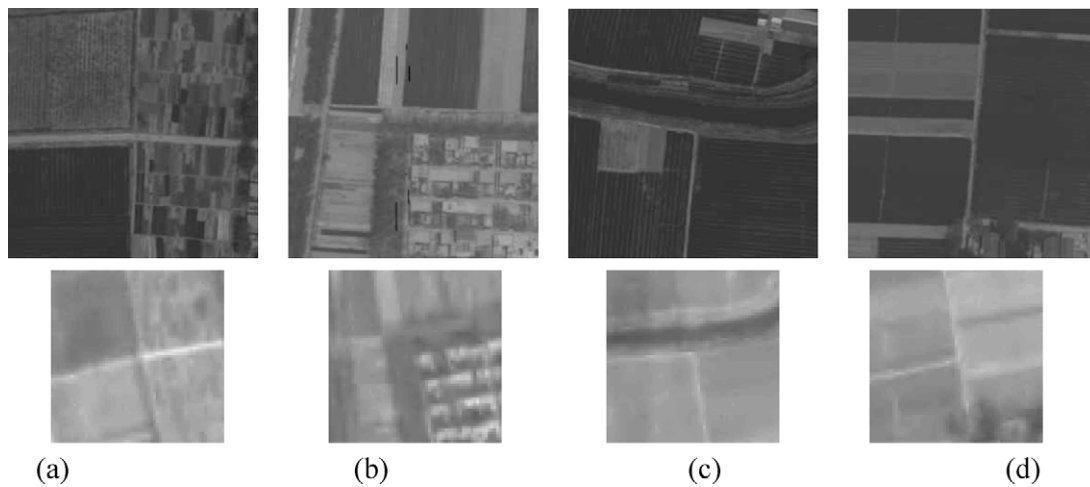


Fig. 1. Top: orthophoto reference images with GCPs; bottom: new images with low spatial resolutions.

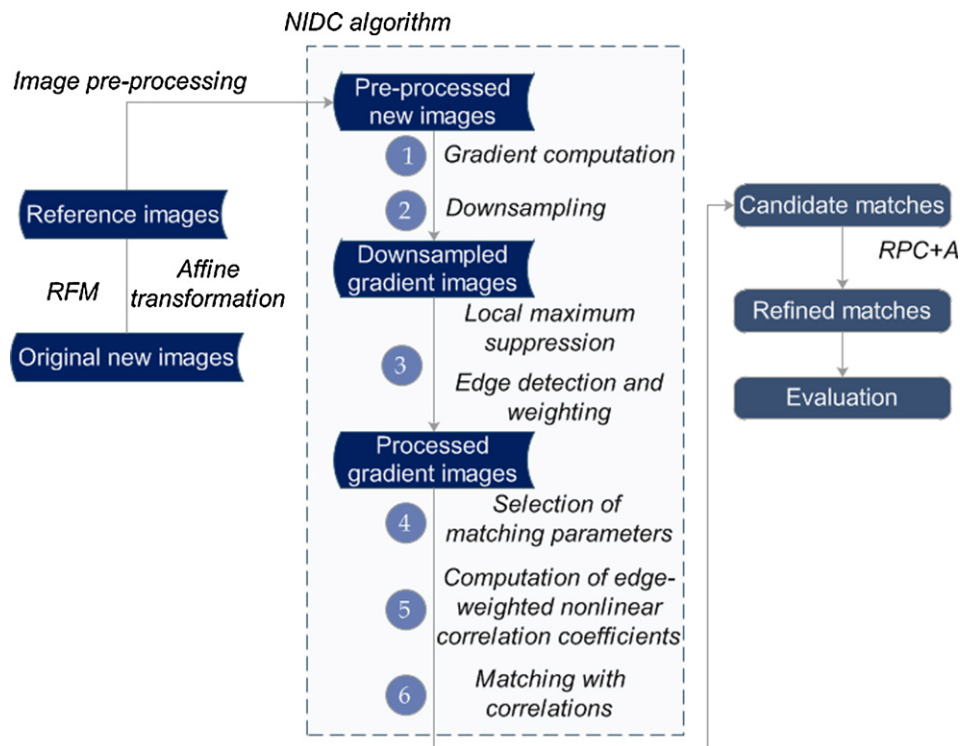


Fig. 2. Work flow of the proposed approach.

after the coordinates of GCPs being converted into WGS84 coordinate system. Errors of original RPC parameters can be obtained from the nominal geo-referencing accuracy information of delivered commercial satellite images. If accuracy information is not available or is simply not good enough, we must manually select 2–3 GCPs to establish geometric relations between reference and new images.

The first step is to roughly register reference and new images. Geometric differences can be rectified using low order polynomial transformation models. For those images having long scanning strips or large coverage areas, they can be segmented based on GCP distribution and multiple sets of polynomial transformation parameters are used for more precise approximation than one single set of parameters. Suppose a GCP has coordinate (x, y) in a reference image, while the point in new image predicted by RPC

is (x', y') . Initial geometric location relations between GCPs and predicted correspondence points can be established by applying an affine transformation:

$$\begin{aligned} x' &= a_0 + a_1x + a_2y \\ y' &= b_0 + b_1x + b_2y \end{aligned} \quad (2)$$

For a GCP (x, y) , a geodetic coordinate system based on the measurement unit of meter is preferred over the longitude and latitude coordinate system since the measurement unit of meter is of a similar size to that of pixels for remote sensing images and possible rounding errors can be avoided. Once we acquire the affine transformation parameters, we can proceed to resample the GCPs in reference images under the premise that center coordinates of the image patches where GCPs are located are preserved

unchanged. With the pre-processing phase, geometric deformations along with resolution disparities (i.e. rotation, scaling and affine differences) can be mostly eliminated. Alternatively, regular image pre-processing techniques including Gaussian filter, linear stretch and Wallis enhancement can be applied to original images before resampling.

2.3. Non-linear intensity difference correlation algorithm

In Section 2.1, we identify one of the major drawbacks of current feature-based matching techniques, which is the lack of robust algorithms that rigorously model non-linear intensity differences. In light of pervasive non-linear illumination variations between multi-temporal remote sensing images, we propose a novel non-linear intensity difference correlation (NIDC) algorithm based on local image gradients. The NIDC algorithm, like mainstream feature detectors, uses edge and gradient features to detect matching candidates. However, the NIDC algorithm further examines the non-linear intensity changes at the pixel level, given detected edge features as principal image matching primitives. The details of NIDC algorithm are given below (also shown in Fig. 2):

- (1) Gradient computation: For each pixel in stereo image pairs, we compute the gradient dx and dy . The derived gradient images (i.e. first order differential images) are less sensitive to the assumption of linear intensity difference, compared with original images. Additionally, we also use the reverse gradients $(-dx, -dy)$ in the feature vector because potential reverse intensity changes may occur for edge features between reference and new images. These reverse gradients are weighted with a small value since intensity reversal is rarely observed, especially for small regions. While SURF extracts the sums of both original and absolute values of Haar wavelet responses in each sub square region of the square window around one interest point, the NIDC algorithm computes the original gradients and their reverses for the entire matching window (not sub-regions).
- (2) Downsampling: Although affine rectifications have been performed for original new images (ref. Section 2.2), we notice that geometric errors still exist. To enhance the robustness to geometric errors, four gradient images $(dx, dy, -dx, -dy)$ are downsampled. Experiments demonstrate that averaging over 3×3 or 4×4 pixels using Gaussian weighted template may produce satisfactory matching results.
- (3) Processing of gradient images: The derived first order differentials manifest themselves as edges in new images. Pixels whose absolute values of gradients are less than 2 are regarded as non-edge regions. For those bright distinct edges, we adopt the strategy of computing “local maximum” as SIFT adopts. Large magnitude gradients are thresholded at a specified value. The filtering of non-edge and the suppressing of over-bright regions further improve capability for the handling non-linear intensity differences.
- (4) Selection of thresholds and weights for edge features: In differential images, edges consist of pixels with large gradient values. In this paper, traditional edge extraction techniques are not employed to detect edge pixels since the detection threshold is difficult to determine for multi-temporal images. There is a risk of losing or wrongly adding edge information in just one image of the pair. Instead, we assume that edge regions normally only take a relatively small part (approximately 5–10% of all pixels) for an image. A ratio of edge pixel number to the overall number of pixels (K) is first selected. Then a histogram-based approach is applied to determine the qualifying threshold of edge pixels (g_0). We can identify edge pixels by checking all pixels against g_0 . Pixel (i, j) whose intensity value is above this threshold is deemed as edge feature and assigned with larger weight w_{ij}

than non-edge pixels as Eq. (3). The weight W quantizes the relative significance of features when computing correlations between reference and new images. Since edge features are more stable than non-edge features, they are assigned with large weights. Typically, non-edge regions are always weighted with 1 while edges are weighted with a value between 10 and 100. We use an analytical approach to choose optimal weights for those edge pixels. Details of weight selection are given in Section 3.3.

$$w_{ij} = W \quad \text{if } g(i, j) \geq g_0$$

$$w_{ij} = 1 \quad \text{if } g(i, j) < g_0 \quad (3)$$

- (5) Computation of edge-weighted non-linear correlation coefficients. The sums of normal and reverse gradients $(\sum dx, \sum dy, -\sum dx, -\sum dy)$ are calculated over each patch in reference and new images using gradient information extracted from each pixel. Based on computed gradient sums, centralized gradients for each image patch can be obtained:

$$\bar{dx} = dx - \frac{1}{mn} \sum dx; \bar{dy} = dy - \frac{1}{mn} \sum dy, \quad (4)$$

where m and n are the length and width of individual image patches. The non-linear correlations between reference and new image patches can be computed by summing up weighted correlation coefficients in both horizontal and vertical directions:

$$\rho = k_1 \rho_x + k_2 \rho_y + k_3 \rho_{-x} + k_4 \rho_{-y} \quad (5)$$

where k_1, k_2, k_3, k_4 are normalization constants to integrate the effects of all four gradient correlation factors $\rho_x, \rho_y, \rho_{-x}, \rho_{-y}$ (corresponding to normal horizontal, normal vertical, reverse horizontal, and reverse vertical gradients respectively). For example, ρ_x is defined as follows:

$$\rho_x = \frac{\sum_{i=1}^m \sum_{j=1}^n \bar{dx} \cdot w_{ij} \cdot \bar{dx}' \cdot w'_{ij}}{\sqrt{\sum_{i=1}^m \sum_{j=1}^n (\bar{dx} \cdot w_{ij})^2} \sqrt{\sum_{i=1}^m \sum_{j=1}^n (\bar{dx}' \cdot w'_{ij})^2}} \quad (6)$$

where \bar{dx} represents the centralized gradient of pixel (i, j) in a reference image patch, \bar{dx}' is the counterpart of \bar{dx} in the new image patch, w_{ij} and w'_{ij} are pixel weighted computed by Eq. (3) for reference and new images respectively. We choose the ratio of k_1 and k_2 according to the ratio between sums of horizontal and vertical gradients in the reference image patches:

$$\frac{k_1}{k_2} = \frac{\sum dx}{\sum dy} \quad (7)$$

For the other two normalized constants, k_3 and k_4 , we need to consider the change information of detected edge features. If two pixels with equal absolute gradient values are opposite to each other, they may belong to the same edge feature. This situation rarely occurs, we usually specify both k_3 and k_4 as a small value such as 0.1. Empirically, k_3 and k_4 should not exceed 0.2. It is different from SURF descriptor, which assigns the same weight to normal gradients values and absolute gradient values. After a distinct weight is assigned to each individual pixel, the non-linear correlations now can be accounted for in our NIDC algorithm.

- (6) Matching with correlations: In this step, we adopt a searching strategy akin to that of traditional gray correlation matching technique, which is performed on a pixel-by-pixel basis. The search window is constrained by initial predict errors of correspondent points, and one can get approximate values through the computation of root mean squared errors (RMSE) during affine transformation by Eq. (2). As for the correlation coefficient threshold, we select 0.5 as our threshold through a large

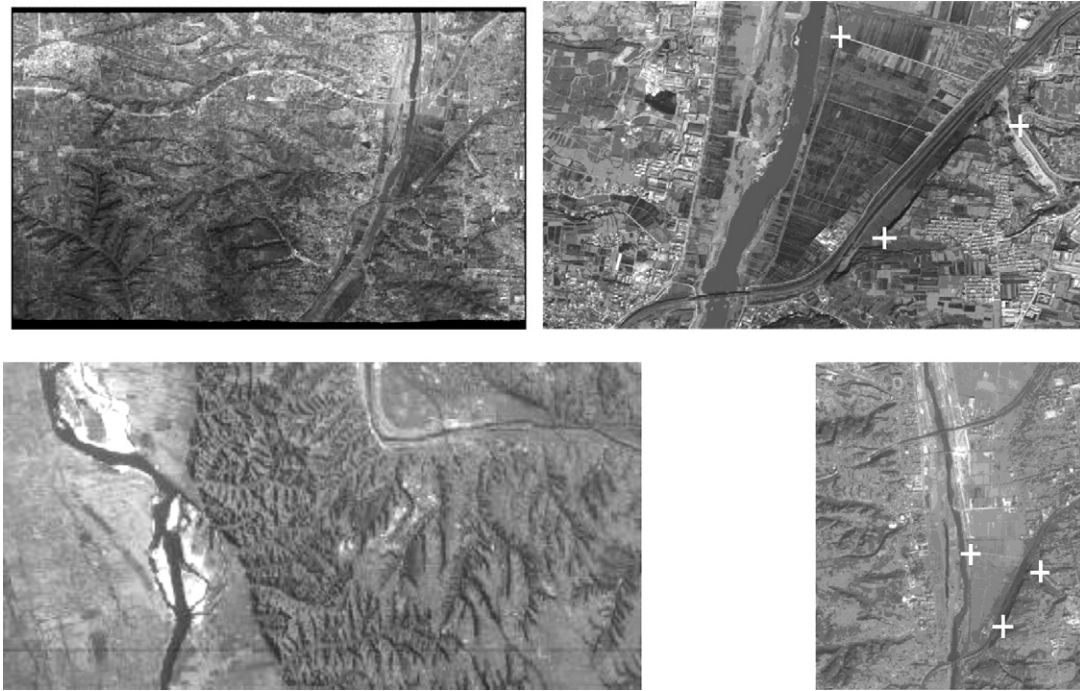


Fig. 3. First test set. Top: reference imagery from ADS40 (left: entire image, right: a zoomed area). Bottom: new imagery from CBERS-02B (left: entire image, right: a zoomed area), matched CPs are indicated as white crosses.

number of tests. Our threshold is lower than traditional thresholds in gray correlation matching because severe radiometric deformations can be observed in our test data. Those pixels with computed correlation scores that are above the threshold are selected as candidate matches.

2.4. Refining of candidate matches

Through the NIDC algorithm, we can obtain a number of candidates of matching CPs. The next step identifies and eliminates false matches from the candidates. Error detection method mainly involves two phases, the identification of geometrical constraints, and the selection of gross error detection algorithms. Being central to image matching accuracy, geometric constraints define geometric models that matching CPs must fit. Common geometric models include approximate epipolar geometry, polynomial fitting, and homology transformation models. These models may not perform well in acquiring accurate and reliable matching results: epipolar constraints can only be used to constrain one-dimensional parallax for stereo image pairs; polynomial fitting models show the disadvantage of low fitting accuracy; and homology transformation is only applicable for plan scenes or near plan situations. In this paper, we assume that information of original RPC parameters and GCP coordinates are already available. And under this assumption, a more restrictive RPC with affine transformation model (hereafter abbreviated as RPC+A) (Fraser et al., 2002) is chosen as our geometric constraint model (Eq. (8)) to remove false matching CPs. Observation error equation can be created as:

$$\begin{aligned} v_x &= f_0 + f_1 \cdot \text{sample} + f_2 \cdot \text{line} - x' \\ v_y &= e_0 + e_1 \cdot \text{sample} + e_2 \cdot \text{line} - y' \end{aligned} \quad (8)$$

where (x', y') are observations of matching points in new images, $e_0, e_1, e_2, f_0, f_1, f_2$, are affine transformation parameters, $(\text{line}, \text{sample})$ are image coordinates of CPs in new images which obtained from Eq. (1).

In terms of gross error detection, the Random Sample and Consensus (RANSAC) algorithm (Fischler and Bolles, 1981) is used in this paper, and the RPC+A model is embedded. After false matches are eliminated, highly accurate image location parameters are obtained at the same time. We can employ parameters of the RPC+A model to evaluate matching accuracy in image space, and the accuracy in object space can be evaluated by the positive solutions of RPC+A and known coordinates of GCPs.

3. Experimental results

3.1. Data

We evaluate the proposed NIDC matching approach with two sets of multi-temporal remote sensing images acquired by different sensors. Each test set consists of several reference images with known GCP coordinates and one new image to be matched. Fig. 3 shows the first test set (I), which consists of reference imagery from Leica ADS40 airborne digital line-scanning sensors (size: $20,001 \times 12,084$ pixel, ground sample distance: 0.5 m) and new imagery from Chinese CBERS-02B satellite (size: $4097 \times 15,000$ pixel, ground sample distance: 2.3 m). Fig. 4 shows the second test set (II) in which 15 aerial photo images taken by film-based frame cameras were used as reference imagery (size per photo: $11,000 \times 11,000$ pixel, ground sample distance: 1 m), and SPOT5 HRS images were used as new imagery (size: $12,000 \times 12,000$ pixel, ground sample distance: 5 m). One can observe considerable geometric and radiometric distortions between reference and new images from the two test sets. Additionally, a number of physical changes of ground objects can be identified. Test set I represents the situation where we can only acquire very sparse GCPs from the reference imagery (totally 46 GCPs), whereas test set II, as shown in Fig. 4, exemplifies an example of spatially dense distribution of GCPs (each photo has approximately 40 feature points as GCPs, totally 706 GCPs). For both test sets, the period between the acquisition of reference and new image data is about 2 years. The two test regions encompass various

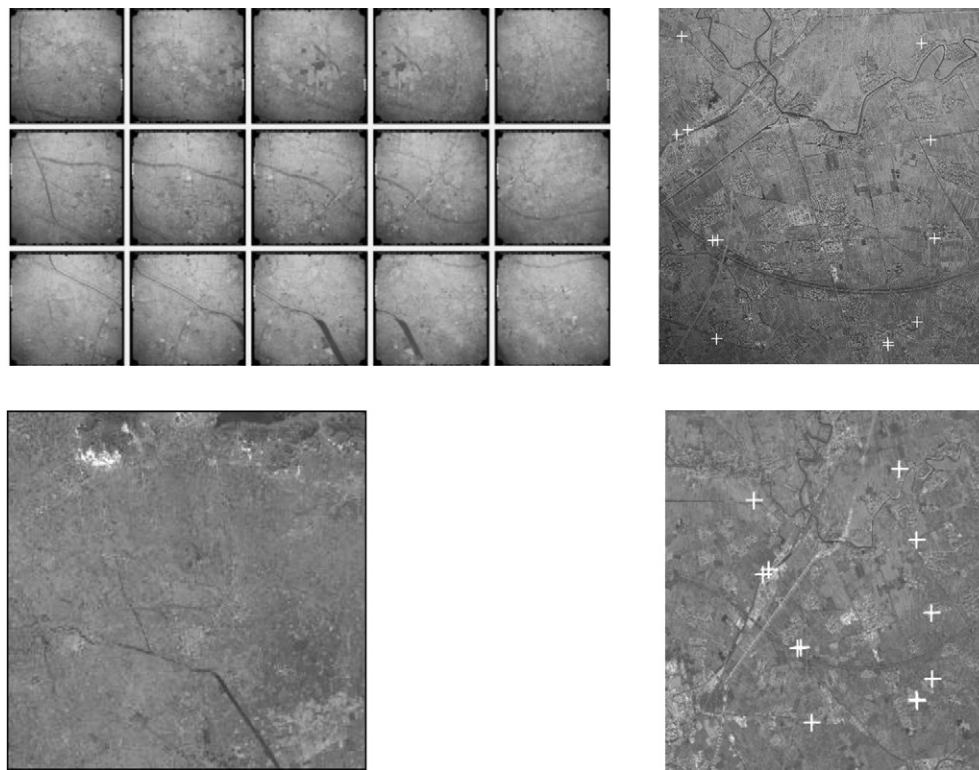


Fig. 4. Second test set. Top: reference imagery from film-based frame aerial photos (left: all 15 images, right: a zoomed area). Bottom: new imagery from SPOT5 HRS (left: entire image, right: a zoomed area).

terrain scenarios, such as mountainous, water, urban, and rural areas. Some land cover changes can be identified in new images. For example, bare land is covered in massive fields of agricultural crops in new images.

3.2. Matching experimental results

The NIDC algorithm was implemented in a C++ dedicated image-matching program. Initially, a total of 46 GCPs were uniformly extracted from the ADS40 reference images over the test filed. Corresponding control points in new CBERS images were then predicted through original RPC parameters by Eq. (1). Then geometric relations between reference images and new CBERS images were approximately established through correspondence points of GCPs with affine transformation in Eq. (2). We further re-sampled the ADS40 reference images according to affine parameters since they have high resolution than new images. NIDC algorithm was then applied to extract a total of 35 GCP matching candidates. The final

refining step produced 31 correct CPs based on the RPC+A model. Similarly, we performed NIDC matching for the second test set, in which 706 CPs were extracted from the SPOT5 reference images. Initial matching produced 244 pairs of CP correspondences. These candidate matches were then filtered using RPC+A model. Finally, we obtained 182 correct matching CPs. In Figs. 3 and 4, some of the final matched CPs (as indicated by crosses) were illustrated. For the two test sets, the comparison results of the proposed matching approach against three common image matching techniques, namely CC, SIFT, and SURF, with respects to matching accuracy in image space, are shown in Table 1.

From Table 1, we can see that after RPC+A refinement, the NIDC algorithm can achieve a RSME as low as 0.69 pixels for SPOTS images in image space. For CBERS, corresponding computed RMSE is about 1.5 pixels, which are considerably better than original RPC prediction accuracy.

In terms of correctly matched CP points, our approach outperforms all other matching methods for both CBERS and SPOTS data

Table 1
Comparison of matching accuracy in image space.

		No. of correctly matched CPs	Root mean squared error (RMSE)		
			x (pixels)	y (pixels)	xy (pixels)
CBERS	Original RPC ^a	46	15.0	18.2	23.6
CBERS	NIDC	31	1.2	0.9	1.54
CBERS	SURF	18	1.28	1.00	1.62
CBERS	CC	13	1.15	1.05	1.55
CBERS	SIFT	25	1.29	1.06	1.67
SPOT	Original RPC ^a	706	1.7	3.8	4.16
SPOT	NIDC	182	0.44	0.53	0.69
SPOT	SURF	88	0.56	0.42	0.70
SPOT	CC	175	0.39	0.48	0.62
SPOT	SIFT	102	0.49	0.51	0.70

^a Original systematic errors before matching.

Table 2
Comparison of positioning accuracy of ground check points by PRC+A model.

		No. of manual CPs	Residual errors		
			N (m)	E (m)	NE (m)
CBERS	Original RPC ^a	10	37.5	45.9	59.3
CBERS	RPC+A	10	3.0	2.4	3.8
SPOT	Original RPC ^a	5	6.1	16.4	17.5
SPOT	RPC+A	5	3.3	3.0	4.4

^a Original systematic errors before matching.

Table 3
Sensitivity analysis of matching parameters.

GCP ID	W = 100			K = 5%		
	K = 5%	K = 10%	K = 20%	W = 1	W = 10	W = 100
8	0.85	0.85	0.88	0.65	0.77	0.85
22	0.55	0.55	0.65	0.26	0.51	0.55
4	0.73	0.72	0.74	0.70	0.72	0.73
5	0.45	0.45	0.47	0.53	0.47	0.45

while the matching performance of SIFT and CC is not stable across the two datasets. Although the CC method can obtain almost the same correct CP points as NIDC on SPOT data, it only finds 13 on CBERS data. Similarly, SIFT has a good performance on CBERS data, but has a poor performance on SPOT data. In general, our NIDC algorithm and matching approach perform consistently better than other common matching techniques in terms of matching success rate. Our approach is demonstrably applicable and robust for multi-sensor and multi-temporal remote sensing images, with either dense or sparse GCPs.

Table 1 shows the geometric matching precision in image space, i.e. internal accuracy. The realistic accuracy of the RPC+A model to reference ground truth, i.e. external accuracy, can be computed based on designated CPs. A number of candidate CP pairs (ten for test set I and five for test set II) that are uniformly distributed were selected as ground check points to estimate external matching accuracy, shown in Table 2.

From Table 2, we can see that the residual errors for SPOT5 and CBERS images are only 4.4 m and 3.8 m respectively in terms of external accuracy, which outperform original RPC location accuracy. The positioning accuracy can meet the requirements of 1:50,000 topographical mapping without extra efforts to establish new CPs in the ground. Experiments also indicate that PRC+A model can be of great use for match refinement and accurate localization with different numbers of GCPs.

3.3. Sensitivity analysis of parameters

The NIDC algorithm encompasses a few critical parameters that should be tuned to achieve satisfactory matching accuracy, including edge pixel ratio (K), feature weight (W), and down-sampling divisions. The down-sampling step is performed over entire images to reduce geometric errors. Experiments demonstrate that the Gaussian weighted averaging of 3×3 or 4×4 sub-regions results in better matching results than other division alternatives, which is similar to what Bay et al. (2008) reported in SURF but with sums of sub-regions. In our experiments, the 4×4 setting was chosen.

Sensitivity analyses were conducted to determine optimal values of K and W . Here we reported our test results in Table 3 using four pairs of CPs shown in Fig. 3. First, we examined the calculated correlation measures coefficients for the four CP pairs by varying K values as 5%, 10%, 20% when W was set to 100. From Table 3, one can observe that the correlation coefficients will be increased as the edge pixel ration K increase, though only slightly. This reveals

that the setting of K is relatively insensitive to the matching stage. Since the extracted edges usually occupy a small fraction in most of common remote sensing images, 5% is adopted as the default value for K . Likewise, the changes of correlation coefficients for CP pairs were evaluated under a fixed K (5%) and varied values of W (1, 10, and 100). When g_0 increases, we can find increases of correlation coefficients in three out of the four CP pairs (Nos. 8, 22, and 4) while the coefficient of No. 5 is decreased. For the No. 5 CP pair, we can see from Fig. 3 that significant changes of its edge features took place in the new image. A larger W thus corresponds to strong correlations between CP pairs if they are correctly matched. Otherwise, a larger W will decrease the correlations if CPs have substantial changes. When W equals 1, which means edge features are not considered, obvious matching errors may occur since edge features are disregarded, as illustrated in No. 22. Based on the preceding sensitivity analyses, the default values of K and W are set as 5% and 100 respectively throughout our experiments.

3.4. Discussion

Different from regular aerial photogrammetric images and close-range images, remote sensing images are collected with various sensors at different dates. The matching of multi-sensor and multi-temporal remote sensing images is then distinct from the counterpart of regular images. While the images are acquired at different times, some features may undergo radiometric or even physical changes. Due to these feature deformations, regular feature-based matching methods perform relatively poorly for remote sensing images acquired using distinct sensors over a long time period. In our NIDC algorithm, traditional feature-based matching approaches are enhanced with the modeling of intensity features during the matching process. We take advantage of initial geometric transformation information between reference image and new images and propose an integrated approach that performs reasonably well in the cases where reference GCPs are either densely or sparsely distributed.

The patches of GCPs are relatively small and may only contain a few features and even less can be extracted. Commonly used matching similarity measure in computer vision that computes the ratio of the distance of the closest neighbor to that of the second-closest neighbor may not be applicable. The adoption of our searching strategy then can avoid this issue.

According to Eq. (6), we compute the correlation coefficient between reference and new images by summing weighted gradient correlation factors in both horizontal and vertical directions, which is similar to SURF. Though, we also use reverse horizontal and vertical gradients with less weights rather than absolute values used in SURF. We believe this configuration is more realistic since two pixels with equal absolute values but are actually having opposite signs are rarely located in the same edge feature. SURF ignores this inequality and may result in many wrong matches most of which are later removed by RANSAC. This explains that our NIDC algorithm can identify more correctly matched CPs than SURF does (as seen from Table 1).

After the accurate transformation parameters are calculated, all the CPs can be projected into new images so as to analyze the GCP changes between reference and new image pairs. To further compare the NIDC algorithm and traditional matching techniques, we compare the correlation coefficients of the NIDC algorithm and traditional matching techniques using the four CPs in Fig. 3.

As seen from Table 4, CC produces relatively low values of correlations due to the linear intensity variation assumption. It is therefore difficult to select an appropriate matching threshold and to determine whether ground object changes really happen or simply the intensity of new images varies. By using SIFT and SURF, one can usually derive relatively high values of correlation coefficients,

Table 4

Comparison of correlation coefficients between NIDC and traditional techniques.

GCP ID	NIDC	SIFT	SURF	CC
8	0.83	0.72	0.78	0.35
22	0.56	0.72	0.80	0.58
4	0.72	0.78	0.72	0.45
5	0.45	0.55	0.69	0.27

which also make it difficult to choose an appropriate threshold to detect true physical changes. The NIDC algorithm is able to detect the true changes of GCPs from the new images. For instance, after we conducted experiments for all matching points, the best threshold of change can be set to 0.5. One can notice that only the patch where No. 5 GCP is located experiences changes. According to close observation, we can verify that physical changes of ground objects have indeed occurred. However, CC may falsely claim Nos. 8 and 4 to be changed GCPs, while SURF and SIFT may wrongly ignore the realistic changes of No. 5 GCP. To summarize, experimental results indicate that our image matching approach has the following advantages:

- (1) Matching accuracy: The achieved matching success rate for available GCPs is marginally better than regular feature-based techniques. As for the other critical internal accuracy measure, RMSE, our approach is also competitive with traditional techniques. In terms of external accuracy, the small residual errors further indicate the superiority of the proposed approach owing to the refining RPC+A model.
- (2) Robustness: Our NIDC algorithm can be readily applicable for many multi-sensor and multi-temporal remote sensing images. A large number of candidate matches and correctly matched GCPs may help reduce overall matching errors and enhance robustness with redundant GCP information. Under the situations where only a small number of GCPs are available, we can still get satisfying matching results. Illumination conditions may vary dramatically between reference and new images and physical changes of ground objects are highly possible over the time. Traditional matching techniques are too rigid to handle these situations.
- (3) Applicability for change detection: Experiments also demonstrate the usefulness of our matching approach for change detection with multi-temporal images. Change detection can be performed along with the image matching tasks at the same time. Small regions where the deformations of edge features take place can be identified with ease. Additionally, our approach can be extended to detect other types of changes that can be reflected in intensity such as the vegetation growth. In such cases, original grayscale images rather than derived gradient images should be adopted for matching.
- (4) Automation: Traditional image matching, triangulation and geo-referencing typically rely on GCPs that are manually selected and created through laborious field work. Obviously, this creates severe operational difficulties given vast quantities of remote sensing data and large terrestrial coverage (Wong and Clausi, 2007). The entire proposed matching approach consists of multiple stages that can be easily automated. Also, since sparse GCPs can guarantee accurate matching results, our approach can significantly reduce or avoid field work on GCP collection.

4. Conclusions and future work

The increasing availability of vast quantitative of multi-sensor and multi-temporal remote sensing images creates challenges to match images in an automatic and robust manner. In response to

the need to handle distinct non-linear intensity imaging conditions, we have introduced a novel automatic robust matching approach for multi-temporal and multi-sensor remote sensing images. In real-world applications, GCPs can be extracted by performing aerial triangulation on reference images that were acquired before. Using these reliable GCPs, the proposed image matching approach can be applied to realize fast yet accurate geo-positioning and reliable change detection for new images in an automatic manner. The essence of our approach is to account for non-linear intensity variations on the basis of extracted gradient features. We have further explored to perform sensitivity analyses to determine the relative strength of intensity features and edge features in the NIDC algorithm. Experimental results demonstrate that the proposed NIDC algorithm perform better than traditional CP matching techniques given densely or sparsely distributed GCPs. Future research will continue this work to find optimized parameter configurations according to available information embedded in matching image sets and to study matching strategies under the situation that RPC or rigid geometric model are unknown.

Acknowledgments

This research was jointly supported by National Basic Research Program of China (Nos. 2012CB719902, 2012CB719906), National Natural Science Foundation of China (Nos. 41023001, 40901190), the Scientific Research Foundation for the Returned Overseas Chinese Scholars, State Education Ministry, P.R. China, and China Western Doctoral Support Project (No. XBBS200809).

References

- Ackermann, F., 1984. High precision image correlation. In: Proceedings of the 39th Photogrammetric Week, Stuttgart, Germany.
- Bay, H., Ess, A., Tuytelaars, T., van Gool, L., 2008. Speed-up robust features (SURF). *Computer Vision and Image Understanding* 110, 346–359.
- Bouziani, M., Goita, K., He, D.-C., 2010. Automatic change detection of buildings in urban environment from very high spatial resolution images using existing geodatabase and prior knowledge. *ISPRS Journal of Photogrammetry and Remote Sensing* 65 (1), 143–153.
- Deilami, K., Hashim, M., 2011. Very high resolution optical satellites for DEM generation: a review. *European Journal of Scientific Research* 49 (4), 542–554.
- Dial, G., 2000. IKONOS satellite mapping accuracy. In: Proceedings of ASPRS 2000, Washington, DC.
- Fischler, M., Bolles, R., 1981. Random sample consensus: a paradigm for model fitting with applications to image analysis and automated cartography. *Communications of the ACM* 24 (6), 381–395.
- Fraser, C., Hanley, H., Yamakawa, T., 2002. High-precision geopositioning from Ikonos satellite imagery. In: Proceedings of ASPRS Annual Meeting, Washington, DC.
- Fraser, C., Hanley, H., 2003. Bias compensation in rational functions for IKONOS satellite imagery. *Photogrammetric Engineering and Remote Sensing* 69 (1), 53–57.
- Holland, D.A., Boyd, D.S., Marshall, P., 2006. Updating topographical mapping in Great Britain using imagery from high-resolution satellite sensors. *ISPRS Journal of Photogrammetry and Remote Sensing* 60 (3), 212–223.
- Li, Q., Zhang, H., Wang, T., 2011. Multispectral image matching using rotation-invariant distance. *IEEE Geoscience and Remote Sensing Letters* 8 (3), 406–410.
- Lowe, D., 2004. Distinctive image features from scale-invariant keypoints. *International Journal of Computer Vision* 60 (2), 91–110.
- Mikolajczyk, K., Schmid, C., 2005. A performance evaluation of local descriptors. *IEEE Transactions on Pattern Analysis and Machine Intelligence* 27 (10), 1615–1630.
- Pacifici, F., Del Frate, F., 2010. Automatic change detection in very high resolution images with pulse-coupled neural networks. *IEEE Geoscience and Remote Sensing Letters* 7 (1), 58–62.
- Peter, R., Rupert, M., Lehner, M., Schroder, M., 2006. Accuracy analysis for DSM and orthoimages derived from SPOT HRS stereo data using direct georeferencing. *ISPRS Journal of Photogrammetry and Remote Sensing* 60 (3), 160–169.
- Tao, C.V., Hu, Y., 2001. A comprehensive study of the rational function model for photogrammetric processing. *Photogrammetric Engineering and Remote Sensing* 67 (12), 1347–1357.
- Wong, A., Clausi, D., 2007. ARRSI: automatic registration of remote-sensing images. *IEEE Transaction on Geoscience and Remote Sensing* 45 (5), 1483–1493.
- Yu, L., Zhang, D., Holden, E.-J., 2008. A fast and fully automatic registration approach based on point features for multi-source remote-sensing images. *Computers and Geosciences* 34, 838–848.
- Zhang, L., Gruen, A., 2006. Multi-image matching for DSM generation from IKONOS imagery. *ISPRS Journal of Photogrammetry and Remote Sensing* 60, 195–211.